ChemComm

Accepted Manuscript

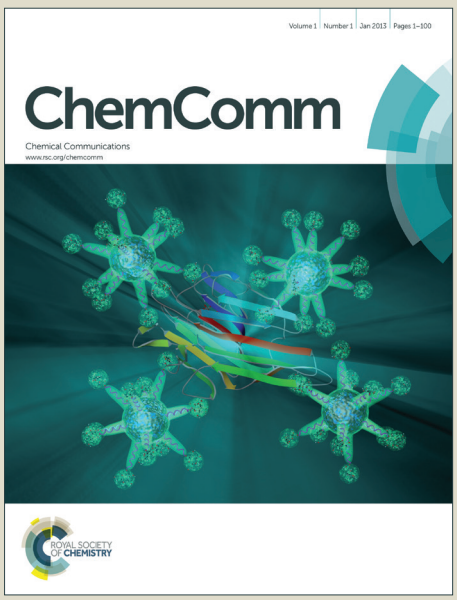

ROYAL SOCIETY OF CHEMISTRY

www.rsc.org/chemcomm

Cite this: DOI: 10.1039/x0xx00000x

Porphyrin photosensitized metal–organic framework for cancer cell apoptosis and caspase responsive theranostics†

Received 00th January 2015,
Accepted 00th January 2015

DOI: 10.1039/x0xx00000x

www.rsc.org/

Lei Zhang, Jianping Lei,* Fengjiao Ma, Pinghua Ling, Jintong Liu and Huangxian Ju*

A photosensitized and caspase-responsive multifunctional nanoprobe was designed by assembling porphyrin, folate targeting-motif and dye-labelled peptide in metal–organic frameworks (MOF) cage, which significantly increases the singlet oxygen quantum yield of porphyrin by 6.2 times, and achieves high efficient cancer therapy and in situ therapeutic monitoring with caspase-3 activation. The integration of theranostic functions in a single nanocarrier holds great promise in precision cancer diagnosis and treatment.

Porphyrin derivatives are most widely applied photosensitizers in photodynamic therapy against a variety of cancers because of their high efficiency in light harvesting and tunable structure.[1] However, the hydrophobicity of many porphyrins results in their aggregation and insufficient tumor localization.[2] To improve the therapeutic efficacy, a well-performing nanocarrier is usually needed to selectively deliver these porphyrin derivatives to tumor targets.[3] Recently, metal-organic frameworks (MOFs), an emerging class of porous materials, have captured prevailing research interest in drug delivery, biosensing and cancer therapy,[4] due to their unprecedentedly large surface area, unique inner porosity and flexible structures.[5] In particular, some porphyrin-based MOFs, which show interesting peroxidase activity, have been used in mimetic catalysis.[6] More recently, Hf^{4+}-porphyrin based MOF has been designed as a highly effective photosensitizer for therapy of resistant head and neck cancer.[7] To enhance the therapeutic efficacy and avoid under- or over-treatment, the integration of theranostic functions in a single nanocarrier is an urgent need in therapeutic monitoring of cancer for precision treatment.

Activatable photosensitizers with intrinsic fluorescence can be developed for therapy and imaging of cancer cells with respect to enzyme expression such as caspase.[8] Caspases are a family of cysteine-aspartic proteases that are only activated during cell apoptosis,[9] and have been used as the sensors for apoptosis imaging and evaluating therapeutic responses.[10] Coupling the apoptosis-inducing capability of photosensitizers with the subsequent caspase activation,[11] the integration of theranostic functions can be achieved in a single nanocarrier. However, the conventional photosensitizers are significantly affected by photobleaching. In view of the structural diversity, tunability and modificability of MOFs to protect both photosensitivity and fluorescence, a multifunctional nanoprobe was here designed for efficient cancer-cell-specific therapy and monitoring the therapeutic effectiveness via caspase-dependent apoptosis imaging (Scheme 1).

The porphyrin derivative, tetrakis(1-methylpyridinium-4-yl)porphyrin (TMPyP), as photosensitizer (PS), could be incorporated in the cage of a variant MOF by one-pot synthesis to form PS@MOF. Interestingly, besides the nanocarrier function and the advantages reported previously,[12] the MOF could significantly increase the singlet oxygen ($^1O_2$) quantum yield of TMPyP by 6.2 times, to efficiently induce cell apoptosis under a laser irradiation. Furthermore, it could quench the fluorescence of Cy3, leading to a caspase-responsive sensing strategy for monitoring cell apoptosis. Thus a Cy3-labelled caspase-3 substrate peptide along with H_2N-PEG-folate (FA) as a target specific moiety could be covalently assembled on PS@MOF surface to perform the sensing and targeting functions. Upon endocytosis of the nanoprobe and laser irradiation, cell apoptosis was encouraged by the therapeutic effect of probe mediated $^1O_2$, and thus activated caspase-3 to specifically cleave the peptide on the probe, which released the Cy3 from MOF surface for fluorescent imaging. The turn-on signal provided an efficient way to image intracellular caspase activity for the real-time evaluation of therapeutic effectiveness.

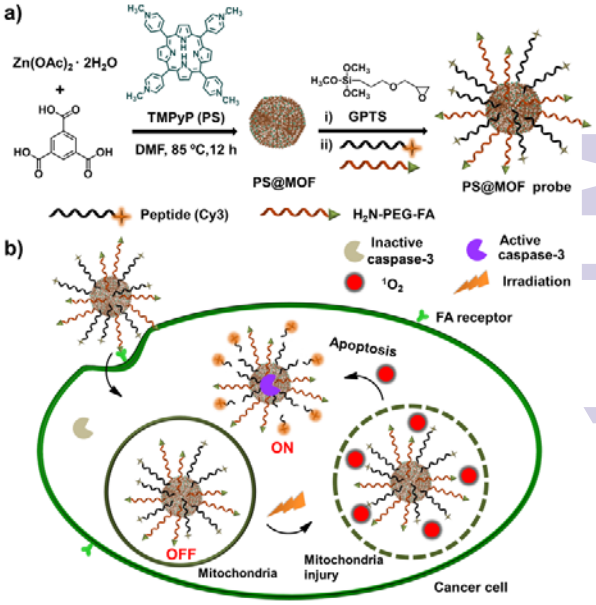

Scheme 1 Schematic representation of (a) PS@MOF probe preparation and (b) FA receptor-targeted delivery of multifunctional PS@MOF probe for cancer cell apoptosis and theranostic with caspase-3 activation.

The transmission electron microscopic (TEM) image of the PS@MOF showed a twisted boracite morphology (Fig. 1a). The nitrogen adsorption-desorption isotherm of PS@MOF gave a micropore size of around 1.50 nm (Fig. S1), closely matching the reported porphyrin-encapsulated variant HKUST-1.[13] The PS@MOF displayed an X-ray diffraction pattern obviously different from that

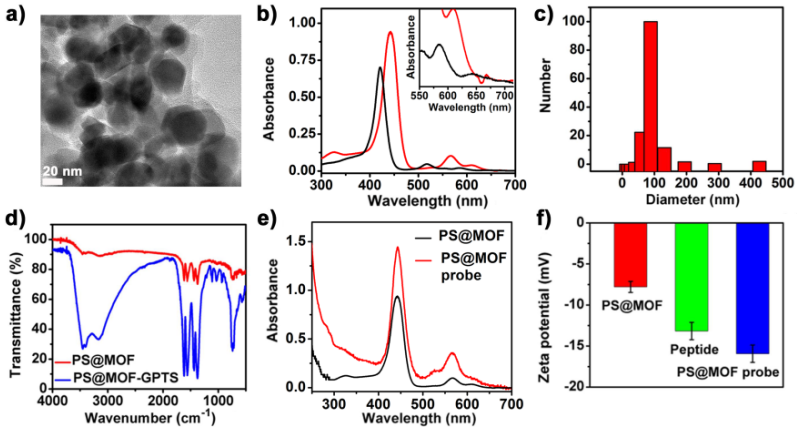

Fig. 1 (a) TEM image of PS@MOF. (b) UV-Vis absorption spectra of TMPyP (black) and PS@MOF (red). Inset: an enlarged view of UV-Vis spectrum of TMPyP and PS@MOF at 550-715 nm. (c) DLS assay of PS@MOF. (d) IR spectra of PS@MOF and GPTS-functionalized PS@MOF. (e) UV-Vis absorption spectra of PS@MOF and PS@MOF nanoprobe. (f) Zeta potential of PS@MOF, caspase-specific peptide and PS@MOF nanoprobe.

of the TMPyP-free MOF (Fig. S2), indicating the existence of TMPyP in the MOF. The encapsulation was proved by the unaltered fluorescence anisotropy curves of TMPyP, which usually changed with the direct interactions between the fluorophores and nanoparticles (Fig. S3).[14] The hydrophobic nature of the MOF cavity led to an obvious bathochromic-shifted Soret-band of TMPyP in the MOF (Fig. 1b).[15] Although the strong absorption of TMPyP in MOF occurred at 442 nm, its NIR characteristic absorption at around 667 nm shifted from 645 nm upon encapsulation in MOF (inset in Fig. 1b) was used as the irradiation wavelength for photodynamic therapy due to its desirable application in living cells. By measuring the absorbance at 420 nm, a loading efficiency of TMPyP in MOF was estimated to be 32.8% (Fig. S4). Dynamic light scattering (DLS) of PS@MOF showed average nanosized hydrodynamic diameter (Fig. 1c), which was beneficial to intracellular assays.

In order to assemble Cy3-labelled caspase-3 substrate peptide and H_2N-PEG-FA on PS@MOF, the surface was firstly functionalized with (3-glycidyloxypropyl)trimethoxysilane (GPTS) to obtain epoxy-terminated PS@MOF-GPTS, which was characterized with a broad band at approximately 1000 cm^{-1} on its infrared (IR) spectrum due to the asymmetric stretching vibration of Si–O group (Fig. 1d).[16] With the typical reaction of epoxy and amino group, the peptide and H_2N-PEG-FA functionalized PS@MOF nanoprobe was obtained to show a new characteristic absorption at around 280 nm and 529 nm (Fig. 1e), which were assigned to FA and Cy3 labeled to peptide, respectively. The surface of PS@MOF nanoprobe showed a more negative potential after modified with electronegative peptide (Fig. 1f), indicating better dispersibility of the nanoprobe in water. The coupling amount of peptide was determined to be 37.1 mg g^{-1} (Fig. S5). The nanoprobe could keep high stability for 30 h in PBS (Fig. S6), which was favorable for the internalization of the nanoprobe by cancer cells via folate receptor (FR)-mediated endocytosis.

The efficient release of $^1O_2$ is a major challenge for photodynamic therapy (PDT) against cancer cells. The $^1O_2$ production under laser irradiation was demonstrated with 1,3-diphenylisobenzofuran (DPBF) as a $^1O_2$ indicator, which could decrease the optical density (OD) at 418 nm upon reaction with $^1O_2$.[17] After individually exposing TMPyP, MOF and PS@MOF solution to a 660-nm irradiation for 210 s, PS@MOF solution showed much greater OD change than free TMPyP, while MOF in the absence of TMPyP generated little variation (Fig. 2a). The surface functionalization of PS@MOF with the peptide and FA did not affect the $^1O_2$ generation. Furthermore, the $^1O_2$ generation dynamics was fast, which trended to the maximum consumption of the indicator at 90 s (Fig. 2a and 2b). Using methylene blue (MB) as a standard, the $^1O_2$ quantum yield (Φ_Δ) could be calculated. It increased from 0.10 ± 0.02 for TMPyP to 0.61 ± 0.05 for PS@MOF under a 660-nm irradiation, indicating the 6.2-times improvement of the photosensitivity of TMPyP by MOF structure.

Considering that the property of excited states is the key factor in the $^1O_2$ generation, a simplified energy level diagram was illustrated in Fig. 2c. The energy level gap of S_1-S_0 for PS@MOF was consistent with TMPyP, derived from the unshifted florescence emission wavelength of TMPyP (Fig. S7a), while the blue-shifted phosphorescent emission of PS@MOF showed a widened difference of T_1-S_0 (Fig. S7b). The narrowed S_1-T_1 gap boosted the intersystem crossing from S_1 to T_1, and the longer average lifetime (τ_P) of T_1 also verified more excited state of PS@MOF in T_1 (Table S1). However, the enhanced intersystem crossing did not necessarily result in the energy transmission from excited PS@MOF toward $^3O_2$ to generate more $^1O_2$, since a competitive relationship existed between $^1O_2$ generation and phosphorescence emission when electrons transfer from T_1 to S_0. The phosphorescence quantum yield (Φ_P) was also measured in Table S1. After encapsulated in MOF, the TMPyP showed the Φ_P of only ~34% that in free state, indicating more energy of excited PS@MOF was transferred to $^3O_2$ to generate $^1O_2$. The high light-harvesting of PS@MOF platform could be attributed to the exact structural match between TMPyP and MOF, which inhibited the free vibration and rotation of the four pyridyl arms, leading to high fluorescence quantum yield (Φ_F) and short fluorescence lifetime (τ_F) (Table S1).[12,13,18]

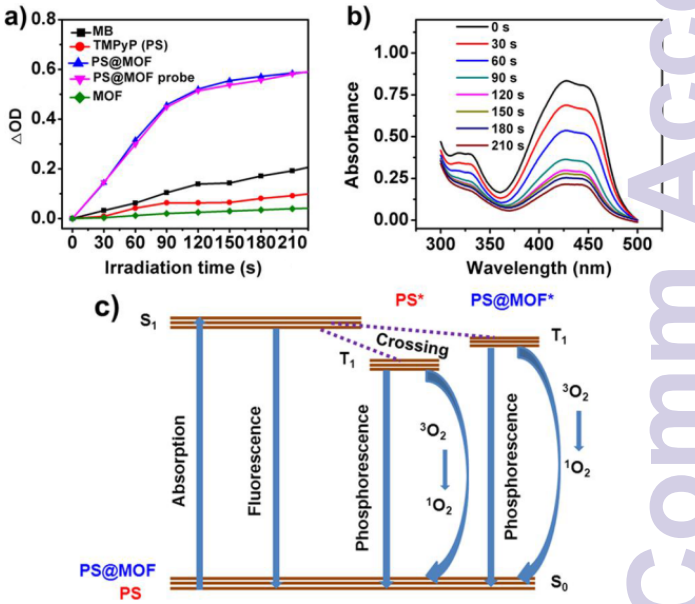

Fig. 2 (a) Plots of change in OD of DPBF (60 μM) in TMPyP (2.0 μM), MOF (1.0 mg mL^{-1}), PS@MOF (2.0 μM, PS equiv.), PS@MOF nanoprobe (2.0 μM, PS equiv.) solution or MB (2.0 μM) as the standard at 418 nm *vs.* irradiation time. (b) Monitoring of $^1O_2$ generated from PS@MOF nanoprobe upon irradiation using DPBF as $^1O_2$ indicator. (c) Modified Jablonski diagram illustrating the process of photosensitized $^1O_2$ production. S_0, singlet ground state; S_1, singlet excited state; T_1, triplet excited state.

To test the validity of the PS@MOF nanoprobe to detect caspase activity, *in vitro* enzymatic assays were performed (Fig. S8). The probe fluorescence was initially quenched via electron transfer from Cy3 to MOF (Fig. S9).[19] At the optimized reaction time of 60 min, the fluorescence intensity linearly increased with the enhancive concentration of caspase-3 to cleave the substrate peptide on the probe, leading to a fluorescent method for detection of caspase-3 activity. The cleavage reaction showed good specificity to caspase against other proteins (Fig. S8), which may interfere with the detection of caspase in living cells. The *in vitro* experiments indicated great potential of the PS@MOF nanoprobe for intracellular caspase activity study.

After 8-h incubation with human cervical carcinoma (HeLa) cells based on FR-targeted endocytosis,[20] PS@MOF nanoprobe was observed to distribute in mitochondria (Fig. S10a-c). Little fluorescent spots were observed in the well growing cells before laser irradiation, indicating caspase was inactive before cell apoptosis. Upon a 660-nm laser irradiation for 15 min, cell apoptosis was encouraged by PS@MOF-mediated $^1O_2$, and Cy3 fluorescence of the nanoprobe was lighted up (Fig. 3a). To clarify the production of reactive oxygen species (ROS) during the irradiation, the nanoprobe-treated HeLa cells were stained with DCFH-DA, a nonfluorescent ROS probe, which was turned to highly fluorescent product upon oxidation by ROS (Fig. S11). Meanwhile, vitamin C as ROS scavenger efficiently reduced the fluorescence of ROS probe. For different postirradiation times, the nanoprobe fluorescence gradually increased with the deepened degree of cell apoptosis (Fig. 3a), indicating that caspase-3 was activated during cell apoptosis and the caspase-activable fluorescence imaging was an effective tool for monitoring the therapeutic efficacy.

The lighted HeLa cells were co-stained with a mitochondrial dye, which showed that the nanoprobe diffused from mitochondrial to cytoplasm after the injury of mitochondria with the laser irradiation (Fig. S10c and S10d). The mitochondrial injury was confirmed by Rhodamine 123 staining,[21] which is readily sequestered by living mitochondria in cells undergoing apoptosis, manifesting the mitochondrial-pathway apoptosis (Fig. S12). In addition, unlike HeLa malignance cells, the nanoprobe-treated human epidermal (HaCat) normal cells, due to the low-level expression of FR, did not show observable fluorescence before and after laser irradiation in confocal imaging and flow cytometric analysis (Fig. S13 and S14).

The specifically caspase-activable fluorescence imaging was confirmed with caspase inhibitor treatment. After caspase-3 inhibitor-pretreated HeLa cells were incubated with PS@MOF nanoprobe and exposed to laser irradiation, the fluorescence was greatly reduced in comparison with that of inhibitor-untreated cells (Fig. 3b). For further verifying the caspase activation during the therapy, a peptide-free probe was synthesized, named as PS@MOF-FA. After incubated with PS@MOF-FA for 8 h and treated with irradiation for 15 min, HeLa cells were collected in lysis buffer after 2-h postirradiation. The cell lysate was then incubated with PS@MOF nanoprobe for fluorescence measurements in a time-dependent manner. A tendency of rapidly increased fluorescence intensity was observed in the absence of caspase inhibitor (Fig. 3c), suggesting that caspase-3 was indeed activated in apoptotic process. Moreover, the caspase-activable fluorescence during cell apoptosis was demonstrated by the TUNEL assay using the additional apoptotic kit (Fig. S15). When HeLa cells were treated with PS@MOF nanoprobe-mediated PDT, the cells showed strong Cy3 fluorescence originating from caspase dependent activation and cleavage, which could be used to monitor therapeutic efficacy.

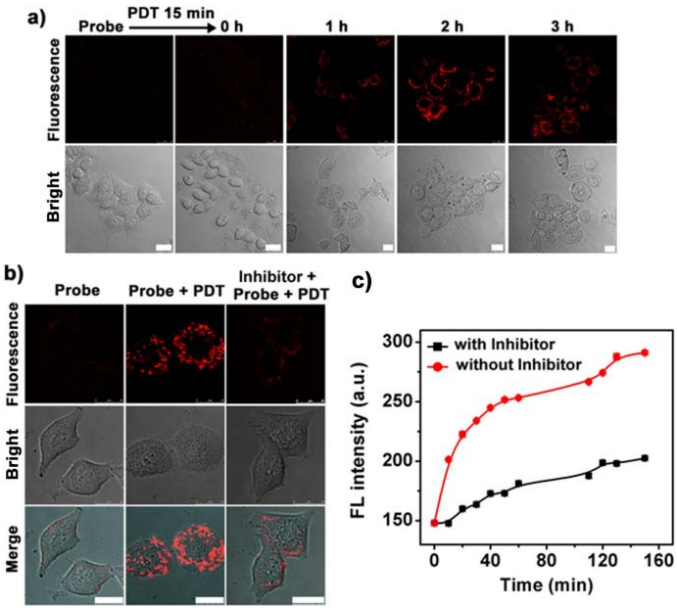

Fig. 3 (a) Confocal imaging monitoring of fluorescence and bright-field of PS@MOF nanoprobe-incubated HeLa cells at different postirradiation times upon irradiation with a 660 nm-laser at 100 mW cm^{-2} for 15 min. Scale bars, 25 μm. (b) Confocal fluorescence imaging of HeLa cells pre-incubated with/without caspase-3 inhibitor during PS@MOF nanoprobe-mediated PDT. Scale bars, 25 μm. (c) Time-dependent fluorescence response of PS@MOF nanoprobe to cell lysate treated with PS@MOF-FA for 8 h and laser irradiation for 15 min

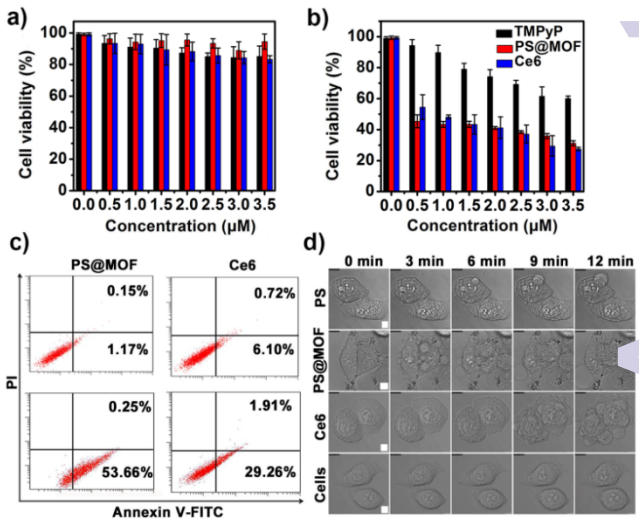

Fig. 4 MTT assays for HeLa cells incubated with PDT agents of different concentrations in the absence (a) and presence (b) of laser irradiation. (c) Flow cytometric analysis of HeLa cells incubated with PS@MOF nanoprobe (0.5 μM, PS equiv.) and Ce6 (0.5 μM) for 8 h before (top) and after (down) laser irradiation for 15 min using apoptosis kit with the dual fluorescence of Annexin V-FITC/PI. (d) Monitoring of morphology change of HeLa cells treated with different PDT agents (1.0 μM) for 8 h and then laser irradiation at 100 mW cm^{-2} for different time. Scale bars, 7.5 μm.

The nanoprobe-caused phototoxicity and therapeutic effectiveness against cancer cells were also evaluated and compared with a conventional photosensitizer, chlorin e6 (Ce6). At each photosensitizer concentration, the cytotoxicity of the correspondingly treated cells was examined using a standard MTT assay (Fig. 4a). Before laser irradiation, these photosensitizers were

little cytotoxic. 8-h incubation with the PS@MOF nanoprobe could maintain about 95% cell viability at the concentrations of 0.5–3.5 μM (PS equiv.), demonstrating low dark-toxicity of PS@MOF nanoprobe. To some extent, PS@MOF nanoprobe was more biocompatible than free TMPyP and Ce6, indicating that MOF could protect TMPyP from biotoxicity. Under a 15-min irradiation with 100 mW cm^{-2} dose, all these reagents exhibited obvious phototoxicity (Fig. 4b). The cell viability of PS@MOF probe- and Ce6-treated HeLa cells was much lower than those treated with TMPyP under the same conditions. Meanwhile, the PS@MOF nanoprobe was more phototoxic than Ce6 at low concentrations, which was confirmed by flow cytometric assays using the Annexin V-FITC/PI apoptotic kit (Fig. 4c). That is, a total 53.91% apoptotic percentage was obtained for PS@MOF nanoprobe-treated HeLa cells, while only 31.17% for Ce6-treated cells at 0.5 μM (PS equiv.). The real-time monitoring was then performed to evaluate the therapeutic effectiveness (Fig. 4d). The morphology of HeLa cells did not change under irradiation for 12 min in absence of photosensitizer. After 3-min irradiation, the PS@MOF nanoprobe-treated HeLa cells began to swell, and more and more bubbles appeared on the surface of cells at a 6-min postirradiation, while the apoptosis characteristics of Ce6-mediated cells occurred after 9-min irradiation, and TMPyP treated-cells did not exhibit significant morphological change. These results demonstrated that PS@MOF nanoprobe with low dark toxicity and high phototoxicity could be considered as a potential photosensitizer for highly efficient therapy against cancer.

In summary, a MOF-based multifunctional nanoprobe has been presented for enhancing the $^1O_2$ quantum yield of TMPyP, triggering the photosensitive cell apoptosis and *in situ* monitoring therapeutic efficacy via caspase-3 activation. The PS@MOF nanoprobe possesses synthetic convenience, good biocompatibility, high phototoxicity for therapy aganist cancer cells and excellent specificity to intracellular caspase-3. The high phototoxicity results from the change of excited level of TMPyP due to its incorporation in MOF cavity. After FR-mediated uptake, the nanoprobe can efficiently generate $^1O_2$ in mitochondria to induce cell apoptosis with caspase-3 activation, which cleaves the peptide for *in situ* imaging of therapeutic efficacy via lighting up the fluorescence of Cy3 labeled to peptide. At relatively low concentration, its therapeutic efficacy is even superior to conventional Ce6. The unique inner porosity, tunable size, modifiable structure and the sensitization of MOF endow the theranostic nanoprobe with promising application in precision cancer treatment.

This research was supported by the National Natural Science Foundation of China (21375060, 21135002, 21121091) and Priority development areas of the National Research Foundation for the Doctoral Program of Higher Education of China (20130091130005).

Notes and references

State Key Laboratory of Analytical Chemistry for Life Science, Collaborative Innovation Center of Chemistry for Life Sciences, School of Chemistry and Chemical Engineering, Nanjing University, Nanjing 210093, P.R. China. E-mail: jpl@nju.edu.cn, hxju@nju.edu.cn. Fax/Tel: +86 25 83593593.

† Electronic Supplementary Information (ESI) available: Experimental details and additional figures. See DOI:10.1039/c000000x/.

1 (a) N. M. Idris, M. K. Gnanasammandhan, J. Zhang, P. C. Ho, R. Mahendran and Y. Zhang, *Nat. Med.*, 2012, **18**, 1580; (b) M. K. Kuimova, S. W. Botchway, A. W. Parker, M. Balaz, H. A. Collins, H. L. Anderson, K. Suhling and P. R. Ogilby, *Nat. Chem.*, 2009, **1**, 69; (c) J. P. Celli, B. Q. Spring, I. Rizvi, C. L. Evans, K. S. Samkoe, S. Verma, B. W. Pogue and T. Hasan, *Chem. Rev.*, 2010, **110**, 2795; (d) M. Ethirajan, Y. H. Chen, P. Joshi and R. K. Pandey, *Chem. Soc. Rev.*, 2011, **40**, 340.

2 M. J. Garland, C. M. Cassidy, D. Woolfson and R. F. Donnelly, *Future Med. Chem.*, 2009, **1**, 667.

3 J. W. Tian, L. Ding, H. X. Ju, Y. Yang, X. Li, Z. Shen, Z. Zhu, J. S. Yu and C. Y. J. Yang, *Angew. Chem., Int. Ed.*, 2014, **53**, 9544.

4 (a) P. Horcajada, T. Chalati, C. Serre, B. Gillet, C. Sebrie, T. Baati, J. F. Eubank, D. Heur-taux, P. Clayette and C. Kreuz, *Nat. Mater.*, 2010, **9**, 172; (b) C. B. He, K. D. Lu and W. B. Lin, *J. Am. Chem. Soc.*, 2014, **136**, 12253; (c) C. B. He, K. D. Lu and W. B. Lin, *J. Am. Chem. Soc.*, 2014, **136**, 5181; (d) A. V. Desai, P. Samanta, B. Manna and S. K. Ghosh, *Chem. Commun.*, 2015, **51**, 6111; (e) H. T. Zhang, J. W. Zhang, G. Huan, Z. Y. Du and H. L. Jiang, *Chem. Commun.*, 2014, **50**, 12069.

5 (a) J. Lee, O. K. Farha, J. Roberts, K. A. Scheidt, S. T. Nguyen and J. T. Hupp, *Chem. Soc. Rev.*, 2009, **38**, 1450; (b) M. O'Keeffe and O. M. Yaghi, *Chem. Rev.*, 2012, **112**, 675.

6 (a) O. K. Farha, A. M. Shultz, A. A. Sarjeant, S. T. Nguyen and J. T. Hupp, *J. Am. Chem. Soc.*, 2011, **133**, 5652; (b) C. Zou, Z. Zhang, X. Xu, Q. Gong, J. Li and C. D. Wu, *J. Am. Chem. Soc.*, 2012, **134**, 87; (c) D. W. Feng, Z. Y. Gu, J. R. Li, H. L. Jiang, Z. W. Wei and H. C. Zhou, *Angew. Chem., Int. Ed.*, 2012, **51**, 10307.

7 K. D. Lu, C. B. He and W. B. Lin, *J. Am. Chem. Soc.*, 2014, **136**, 16712.

8 J. F. Lovell, T. W. B. Liu, J. Chen and G. Zheng, *Chem. Rev.*, 2010, **110**, 2839.

9 (a) D. J. Ye, A. J. Shuhendler, L. N. Cui, L. Tong, S. S. Tee, G. Tikhomirov, D. W. Felsher and J. H. Rao, *Nat. Chem.*, 2014, **6**, 519; (b) J. F. Lo, M. W. Chan, Q. C. Qi, J. Chen and G. Zheng, *J. Am. Chem. Soc.*, 2011, **133**, 18580; (c) Y. Y. Yuan, R. T. K. Kwok, B. Z. Tang and B. Liu, *J. Am. Chem. Soc.*, 2014, **136**, 2546.

10 (a) H. B. Wang, Q. Zhang, X. Chu, T. T. Chen, J. Ge and R. Q. Yu, *Angew. Chem., Int. Ed.*, 2011, **50**, 7065; (b) X. L. Huang, M. Swierczewska, K. Y. Choi, L. Zhu, A. Bhirde, J. Park, K. Kim, J. Xie, Z. Niu, K. C. Lee, S. Lee and X. Y. Chen, *Angew. Chem., Int. Ed.*, 2012, **51**, 1625; (c) Y. Z. Min, J. M. Li, F. Liu, E. K. L. Yeow and B. G. Xing, *Angew. Chem., Int. Ed.*, 2014, **53**, 1012; (d) H. B. Shi, R. T. K. Kwok, J. Z. Liu, B. G. Xing, B. Z. Tang and B. Liu, *J. Am. Chem. Soc.*, 2012, **134**, 17972.

11 K. Stefflova, J. Chen, H. Li and G. Zheng, *Mol. Imaging*, 2006, **5**, 520.

12 J. Park, D. Feng, S. Yuan and H. C. Zhou, *Angew. Chem., Int. Ed.*, 2015, **54**, 430.

13 Z. J. Zhang, L. P. Zhang, L. Wojtas, M. Eddaoudi and M. J. Zaworotko, *J. Am. Chem. Soc.*, 2012, **134**, 928.

14 Q. B. Wang, W. Wang, J. P. Lei, N. Xu, F. L. Gao and H. X. Ju, *Anal. Chem.*, 2013, **85**, 12182.

15 R. W. Larsen, J. Miksovska, R. L. Musselman and L. Wojtas, *J. Phys. Chem.*, 2011, **115**, 11519.

16 S. Chen, A. Osaka, T. Ikoma, H. Morita, J. Li, M. Takeguchi and Y. Hanagata, *J. Mater. Chem.*, 2011, **21**, 10942.

17 N. Adarsh, R. R. Avirah and D. Ramaiah, *Org. Lett.*, 2010, **12**, 5720.

18 (a) H. J. Son, S. Jin, S. Patwardhan, S. J. Wezenberg, N. C. Jeong, M. So, C. E. Wilmer, A. A. Sarjeant, G. C. Schatz, R. Q. Snurr, O. K. Farha, G. P. Wiederrecht and J. T. Hupp, *J. Am. Chem. Soc.*, 2013, **135**, 862; (b) J. Zhang and M. J. Zaworotko, *Chem. Soc. Rev.*, 2014, **43**, 5444; (c) J. R. Lakowicz, *Principles of Fluorescence Spectroscopy*, Springer 3rd edn., 2006, ch. 1, pp. 8–10.

19 X. Zhu, H. Y. Zheng, X. F. Wei, Z. Y. Lin, L. Guo, B. Qiu and G. N. Chen, *Chem. Commun.*, 2013, **49**, 1276.

20 (a) S. Nayak, H. Lee, J. Chmielewski and L. A. Lyon, *J. Am. Chem. Soc.*, 2004, **126**, 10258; (b) P. Huang, C. Xu, J. Lin, C. Wang, X. Wang, C. Zhang, X. Zhou, S. Guo and D. Cui, *Theranostics*, 2011, **1**, 240.

21 P. M. Kasili, J. M. Song and T. Vo-Dinh, *J. Am. Chem. Soc.*, 2004, **126**, 2799.